Case Studies in Construction Materials 17 (2022) e01568

Contents lists available at ScienceDirect

Case Studies in Construction Materials

journal homepage: www.elsevier.com/locate/cscm

Case study

Experimental and analytical study for shear strengthening of reinforced-concrete beams using a prefabricated geopolymer–mortar panel

Rita Irmawaty [a,*], Fakhruddin [a], Januarti Jaya Ekaputri [b]

[a] Department of Civil Engineering, Faculty of Engineering, Universitas Hasanuddin, Makassar 92171, Indonesia
[b] Civil Engineering Department, Faculty of Civil, Planning, and Geo-Engineering, Institut Teknologi Sepuluh November, Surabaya, Indonesia

ARTICLE INFO

Keywords:
Anchor bolt
Geopolymer mortar
Shear strengthening

ABSTRACT

This study investigated the performance of geopolymer–mortar panels (GMPs) in improving the shear capacity of reinforced-concrete (RC) beams. A GMP with a thickness of 15 mm was prefabricated and fixed to the shear span of beams using mechanical anchors. Five RC beams were constructed and tested under a four-point bending monotonic load: one unstrengthened, three strengthened with a GMP, and one strengthened with a Portland-cement-mortar panel. The investigated parameters included (a) anchor-bolt spacing, (b) presence of a wire mesh, and (c) binding material types. The results indicated that the GMP is an effective technique for improving the shear capacity of RC beams. The maximum gain in the shear capacity of the strengthened beams ranged from 14.1% to 34.9% with respect to the unstrengthened beam. Moreover, the results suggested that the failure mode of the beam changed from brittle to ductile failure if an anchor bolt spacing of 200 mm and wire mesh were used at the GMP. Based on these findings, the GMP can be used as an alternative method for shear-strengthening RC beams in building applications owing to its high strength and ductility. Finally, an analytical model based on the simplified-modified–compression-field theory model was proposed to predict the shear capacity of RC beams strengthened with the GMP. The analytical model was in reasonable agreement with the test results.

1. Introduction

One of the relevant countermeasures for enhancing the performance of existing RC structures to meet standard requirements is the strengthening method. Several techniques are often adopted, such as the bonded-external–steel-plate method, which significantly contributes to structural enhancement. However, its disadvantages include corrosion and fire resistance. A popular approach is Fiber Reinforced Plastic (FRP), which is characterized by a high strength-to-weight ratio, ease of application, adequate corrosion resistance, and minimization of the change in geometry. However, owing to its poor resistance to high temperatures [1], inefficient application in moist environments, incompatibility with concrete substrates, and the probability of abrupt failure without warning [2], this material is not deemed suitable. All these issues are due to the organic resin used to bond the fibers in the FRP (epoxy).

An innovative strengthening method known as a geopolymer–mortar panel (GMP) offers a promising solution to these issues. A

* Corresponding author.
E-mail address: rita_irmaway@yahoo.co.id (R. Irmawaty).

https://doi.org/10.1016/j.cscm.2022.e01568
Received 23 July 2022; Received in revised form 28 September 2022; Accepted 11 October 2022
Available online 13 October 2022
2214-5095/© 2022 The Author(s). Published by Elsevier Ltd. This is an open access article under the CC BY license (http://creativecommons.org/licenses/by/4.0/).

Nomenclature

A_c	cross-sectional area of concrete
A_{sl}	cross-sectional area of the longitudinal rebars
a_g	Maximum size of coarse aggregate
b	width of beam
b^*_w	width of the base of the concrete semi-pyramidal tensile fracture
d	effective depth
E_s	elastic modulus of steel
E_{wire}	modulus elastic of wire mesh
f'_c	compressive strength of concrete
$f_{st.y}$	yield stress of transverse rebars
h	height of beam
h_{panel}	height of the panel
I	second moment of area
S_{xe}	crack spacing parameter
t_{panel}	panel thickness
V	shear force
Vc	shear force in concrete
Vs	shear force in transverse rebars
Q	first moment of area
v	shear strength
v_c	shear strength in concrete
v_s	shear strength in transverse reinforcement
v_{wire}	shear strength in wiremesh
v_{panel}	shear strength in panel
a	angle defining the concrete fracture surface
β	factor accounting for the tensile stress in the cracked concrete
θ	direction of the principal stress/strain
ρ_{st}	stirrups ratio
ρ_{sx}	reinforcement ratio of longitudinal reinforcement
ρ_{sl}	Longitudinal steel reinforcement ratio
ρ_{wire}	ratio of transverse wiremesh
τ_{max}	maximum shear stress in a rectangular non-cracked section
τ_{avg}	average shear stress of the panel
ε_x	yield strain of longitudinal reinforcement
ε_{wire}	effective strain of wire mesh
ε_{sl}	longitudinal strain assessed at a mid-depth of the beam cross section
s_x	yield strain of longitudinal reinforcement

GMP is a 15 mm panel made of fly-ash based geopolymer mortar that is mechanically anchored to the shear span of beams. In the South Sulawesi Province, Indonesia, there is a large amount of fly-ash waste from steam-power plants. Unused fly-ash waste has immense potential as a construction material for producing geopolymer mortar or concrete.

Geopolymer mortar/concrete was proposed by Davidovits [3], and it is described as a non-cement material manufactured from alkali-activating aluminosilicates, including industrial wastes (fly ash and blast-furnace slag) or metakaolin at low calcination temperatures [4–12]. Studies on geopolymers and activated-alkali materials have revealed that their properties are comparable or superior to those of OPC mortar or concrete [13–18]. Owing to their superior mechanical properties, good resistance to high temperatures, and corrosion resistance, geopolymers are regarded as viable substitutes for cement in building construction [10,19].

One of the main limitations of geopolymer mortars that should be overcome for large-scale structural applications is inherent brittleness. Some studies have been conducted on fly-ash based geopolymer composites reinforced with various fibers; these fibers include polypropylene [20–25], cotton [26], glass [27], natural flax [28], carbon [15,29], basalt [16], steel [16,17,30–34], and polyvinyl alcohol (PVA) [35,36]. According to Ekaputri et al. [35], PVA fibers can improve the strength, ductility, and workability of geopolymer mortars. Therefore, PVA fibers were used in the present study.

Studies on geopolymer mortars have been extended to various applications in RC structures, such as strengthening materials for RC beams. Many studies have been conducted to investigate the use of geopolymer mortars as flexural strengthening materials for RC beams [37–43]. Experimental results showed an increase in the maximum load capacity and stiffness owing to the tensile capacity and higher bond strength of the geopolymer mortar and reinforcement. For shear strengthening, Zhang et al. [44] used a textile-reinforced geopolymer mortar (TRGM) as the strengthening material for RC beams. Test results showed that one and two layers of TRGM increased the shear capacity by 47% and 106%, respectively, when compared to the unstrengthened beam. In their study, the beam

was shear strengthened using a U-shaped TRGM and bonded with a geopolymer mortar. In this study, geopolymer–mortar panels were prefabricated (precast) and applied as structural elements using anchor bolts. This prefabricated panel has advantages over the cast-in-place method used by Zhang et al. [44], such as more quality control and faster implementation. In addition, shear strengthening of RC beams using geopolymer–mortar panels have not been previously conducted. A similar method has been conducted using different materials, such as ultra-high-strength–fiber-reinforced concrete [45], mortar reinforced with recycled-steel fibers [46], and mortar reinforced with CFRP laminates [47].

Therefore, this study investigated the shear performance of RC beams strengthened with a 15-mm-thick GMP anchored to both sides of the RC beams. This is expected to improve the structural performance of RC beams, such as shear capacity, stiffness, ductility, and failure mode. The feasibility of a GMP as a shear strengthening method was evaluated, and the effects of the anchoring spacing, wire mesh, and binding materials were discussed. Finally, a modified prediction model is proposed to evaluate the shear capacity of the strengthened RC beams.

2. Experimental program

2.1. Specimens and parameters

The experimental program investigated the performance of a GMP as a shear strengthening method in RC beams subjected to static monotonic loading. As shown in Fig. 1, a beam with cross-section of 150 × 300 mm and length of 2300 mm was fabricated and tested as simply supported in a symmetric four-point load setup.

The same batch of ready-mix concrete was used to produce all the beams with a compressive strength of 25 MPa. Meanwhile, the actual compressive strength at 28 days was 27.5 MPa measured on 100 × 200 mm cylinders. The beams were reinforced in the tension and compression zones with three and two longitudinal rebars of 16 and 10 mm diameters, respectively. Stirrups with 10–350 and 10–300 mm diameters, were arranged in the shear span and constant-moment regions, respectively. The properties of reinforcing steel are listed in Table 1. The control beams were designed to fail in shear, allowing the flexural resistance to exceed the shear resistance. To ensure the occurrence of shear failure, a cross-sectional analysis of the flexural and shear capacities was conducted. The calculation results showed that the flexural and shear capacities of the beams were 159.9 kN and 125.5 kN, respectively. This indicated that the flexural capacity of the beam was higher than the shear capacity. Therefore, the failure mode is shear failure.

Four beams were shear strengthened at the shear span, and one beam was tested without shear strengthening as a control beam (Table 2). The parameters of this study included (a) anchor bolt spacing (200 and 300 mm), wire mesh (with and without a wire mesh), and binding material (geopolymer mortar and Portland-cement-mortar). Three beams were strengthened using a geopolymer–mortar panel and one with a Portland-cement-mortar panel.

The control and strengthened beams are denoted as CB and X-Y-Z, respectively. X in the strengthened beams indicates the type of binding material (GM for geopolymer mortar and PC for Portland-cement-mortar), Y is the presence of wire mesh (W for wire mesh and NW for no wire mesh), and Z denotes the anchor bolt spacing (200 and 300 mm). The details of the tested beams are tabulated in

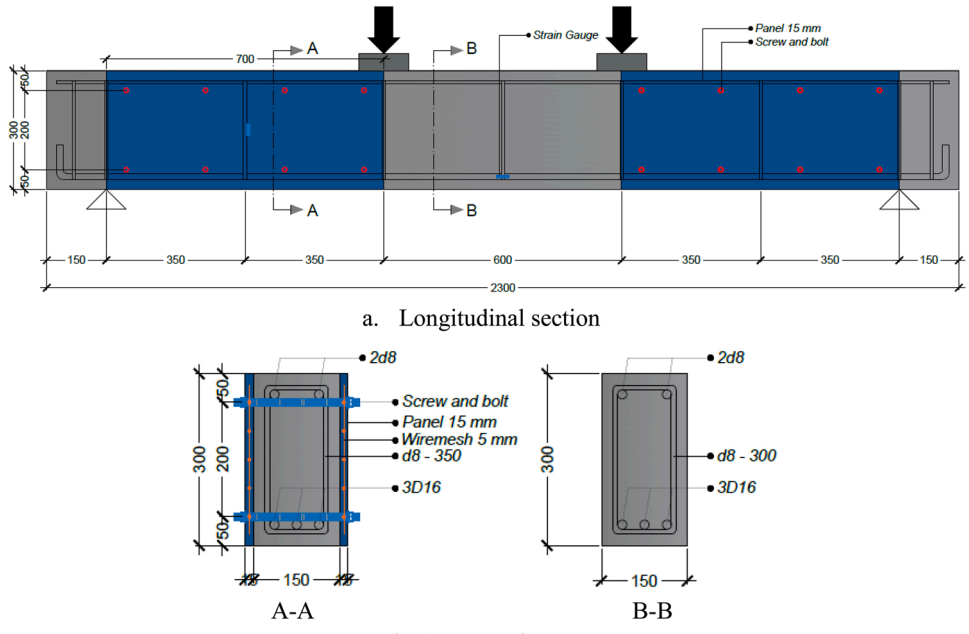

Fig. 1. Geometry and detail of beam (unit in mm).

Table 1
Properties of reinforcing bars.

Reinforcement	Diameter (mm)	A_s (mm^2)	f_y (MPa)
Tension	16	200.96	384.8
Compression	8	50.24	336.7
Stirrup	8	50.24	336.7
Wire mesh	5	19.63	490.0

Table 2
Beam variations.

Specimens	Binding material of panels	Bolt spacing (mm)	Wire mesh
CB	–	–	–
GM-W-200	Geopolymer mortar +PVA	200	5 mm
GM-W-300	Geopolymer mortar +PVA	300	5 mm
GM-NW-200	Geopolymer mortar +PVA	200	–
PM-W-200	Portland-cement-mortar + PVA	200	5 mm

Table 2, and the panels, including anchor bolt spacings and wire mesh, are shown in Fig. 2.

The longitudinal spacing between anchor bolts was determined based on the angle of the shear plane (θ), which normally varies between 22° and 45° for normal-strength concrete. As shown in Fig. 2a, the transverse spacing between anchor bolts was 200 mm. The longitudinal spacing between the anchor bolts were calculated using Eq. (1).

$$\text{Longitudinal } spacing = \frac{\text{Transverse } spacing}{\tan\theta} \tag{1}$$

With a transverse spacing of 200 mm and shear plane (θ) between 22° and 45°, a longitudinal spacing between bolts of 200 and 495 mm was obtained. The bolts were arranged as uniformly as possible along the length of the panel. Therefore, the longitudinal spacing between the bolts in this study was 200 and 300 mm.

2.2. Binding materials

GM was produced using low-calcium fly ash (FA) obtained as a waste product from coal power plants. The chemical composition of FA was obtained by conducting X-ray fluorescence (XRF) tests, and the results are presented in Table 3. The total chemical composition of $SiO_2 + Al_2O_3 + Fe_2O_3$ was 60.07%. Thus, according to ASTM C 618, the FA used in this study was Class C.

GM was used as the binding material for the strengthening panels in the GM-W-200, GM-W-300, and GM-NW-200 beams. It was prepared using 25% FA, 25% alkali, 50% sand, 1.5% borax, and 2% superplasticizer. A 0.6% PVA fiber by the total mixture was added. The activator solution consists of sodium hydroxide (NaOH) 8 M. The ratio of NaOH to sodium silicate (Na_2SiO_3) was 1.5. NaOH 8 M was obtained by dissolving 320 g of solid NaOH in aquades until it reached 1 liter. Therefore, the aquades requirement for a 1 m^3 GM was approximately 132.6 L/m^3 as shown in Table 4.

The mixing procedures for GM were as follows: FA and fine aggregates were mixed in a standard pan mixer for two minutes. The alkali activator was then poured into the mixture and mixed for two minutes. Superplasticizers were added to improve the workability of the geopolymer matrix, and the fibers were gently combined and blended until a uniform dispersion was obtained. The flow rate of the fresh geopolymer was 235 mm. The freshly mixed geopolymer mortar was then poured into molds to fabricate the GMP.

A universal testing machine was used to determine the compressive strength of the GM with a cube size of 50 × 50 mm. The splitting-tensile strength was tested on cylindrical specimens of dimensions 50 × 100 mm. A universal testing machine with a capacity of 1000 kN was used to determine the compressive strength of the GM with a cube size of 50 × 50 mm. The loading rate of the

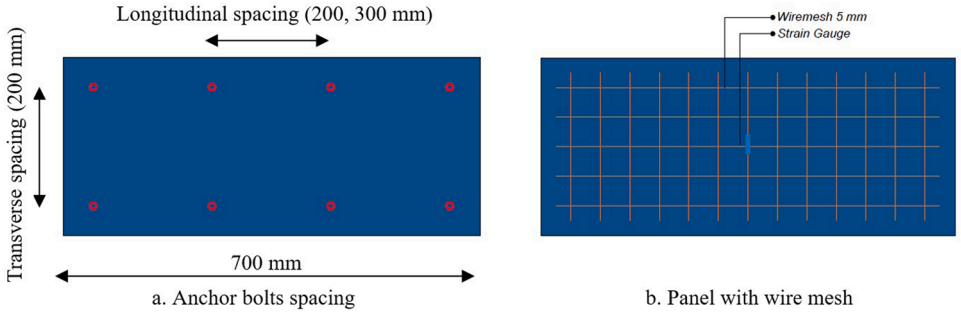

Fig. 2. Strengthening panel.

Table 3
Chemical composition of FA based on XRF test (% by weight).

SiO_2	Al_2O_3	Fe_2O_3	CaO	Na_2O	K_2O	MgO	H_2O	SO_3
37.04	11.41	11.62	19.24	0.57	0.72	4.53	0.51	1.37

Table 4
Mix proportion of GM and PM (kg/m^3).

Binding material	FA	Cement	Water	NaOH	Na_2SiO_3	Sand	Plasticizer	PVA
Geopolymer mortar	390	–	132.6	156	234	780	7.8	6.5
Portland-cement-mortar	–	636	299	–	–	1360	–	4

compressive strength test was 0.2 MPa/s based on the ASTM C39/C39M-01 standard test method for the compressive strength of cylindrical concrete specimens.

For comparison, commercial Portland cement (PM) was used to fabricate the strengthening panel, and its compressive design strength was similar to that of the GM. The dimensions of the specimens used to determine the compressive and tensile strengths of PC were also similar to those of GM. The mix proportions of GM and PM are presented in Table 4. The water to cement (w/c) ratio of the Portland-cement-mortar mix of 299 kg/m^3 is also presented in this table.

2.3. Fabrication procedures

Geopolymer and Portland-cement-mortar panels were fabricated. The process started with the installation of a wooden formwork, marked with the location of the bolt holes using a PVC pipe with a diameter of 0.5 inch (12.5 mm), as shown in Fig. 3a. After curing for 24 h, the GMP was removed from the formwork. Subsequently, moist curing was continued for 28 days by wrapping with wet laps and covering with plastic bags. A similar procedure was adopted for the PC-mortar panel.

This process led to the fabrication of RC beams. After 28 days of curing, the three beams were strengthened with a geopolymer–mortar panel at the shear span, one beam was strengthened with a Portland-cement-mortar panel, and the remaining one was left unstrengthened to represent the control specimen.

Before strengthening, the beams were prepared by grinding the surfaces and edges until any loose material was removed. Subsequently, strengthening panels were placed on each side of the beams at the shear span. The panels were fixed to a concrete substrate with anchors composed of bolts and nuts on both sides (Fig. 3b).

2.4. Test setup

All beams were subjected to monotonic loads under a 4-point load setup with a total and shear span of 2000 and 700 mm, respectively. Furthermore, the loads were monitored using a load cell and increased monotonically in the displacement-control mechanism of 0.2 mm/s. One side of the beam was painted white to observe cracking. After each load level was reached, any cracks formed during loading were marked and photographed. The loading test environment is shown in Fig. 4.

The deflections at the midspan and under the loading points were recorded using three linear-variable–displacement-transducers (LVDT). To facilitate control of the potential yield for steel bars, a strain gauge was attached to the tensile–longitudinal rebars at the midspan, whereas the other gauge was bonded to the stirrups at the shear span. Fig. 5 shows the Phi-gauges attached at the interface between the panel and RC beam to evaluate compatibility. The data from the load cell, displacement transducers, phi-gauge, and strain gauges were recorded using a data logger. Finally, two digital cameras were used to capture the crack patterns on both sides of the beam until failure.

a. Fabrication of GM panels b. Installation of panels into RC beam

Fig. 3. Fabrication procedures.

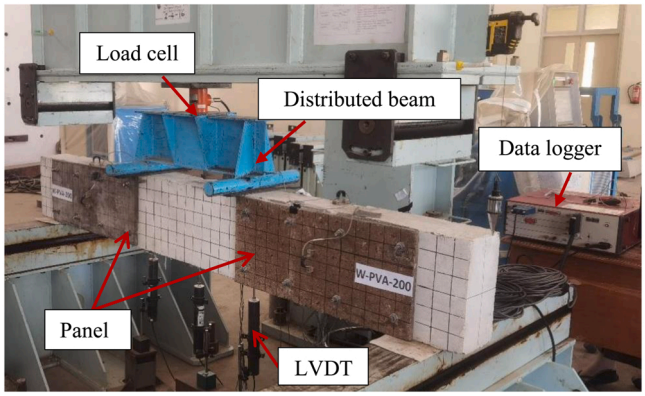

Fig. 4. Setup of the loading test.

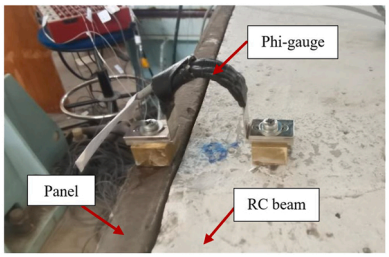

Fig. 5. Phi-gauges at the interface between the RC and panel.

3. Test results and discussion

3.1. Compressive and splitting-tensile strengths

From Table 5, the compressive and splitting-tensile strengths of the GM with PVA fibers at 28 days was 21.5 MPa and 2.1 MPa, respectively. Meanwhile, the compressive and splitting-tensile strengths of a Portland-cement mortar with PVA fibers at 28 days was 23.2 MPa and 2.5 MPa, respectively. The results indicate that the compressive and splitting-tensile strengths of the GM were similar to those of the PC mortar.

3.2. Load–displacement response

Displacement at the midspan was monitored during the loading test. The data was used to evaluate the stiffness variations in the beams. Fig. 6(a–c) present the effect of anchor-bolt spacing, wire mesh and binding material on the load–displacement behavior. A summary of the cracking load, yielding load, failure load, and failure mode for each beam is presented in Table 6. It can be seen from Fig. 6 that the stiffnesses of all the beams were similar, prior to the dominant diagonal crack which formed at a load of 115 kN. The stiffness of the control beam decreased significantly after this stage, until failure. However, the stiffness of the strengthened beams also increased. This is because the strengthening panel resisted part of the shear load and stopped further diagonal crack propagation.

In this study, displacement control was used during the loading process, resulting in a descending branch of the load–deflection curve. The descending behavior revealed that the control beam (CB), GM-W-300, and GM-NW-200 experienced brittle failure, where the load suddenly dropped at failure. Meanwhile, the remaining beams (GM-W-200 and PM-W-200) exhibited ductile behavior, where the load slightly decreased at failure.

The effect of anchor-bolt spacing was observed in the post-yield behavior, where GM-W-200 continuously deformed until the ultimate load, whereas GM-W-300 immediately collapsed (Fig. 6a). The wire mesh significantly improved the maximum load and displacement of the beams (Fig. 6b). Meanwhile, with the effect of the binding materials (Fig. 6c), the load–deflection behavior was

Table 5
Compressive and splitting-tensile strengths at 28 days.

Binding materials	Compressive strength (MPa)	Splitting-tensile strength (MPa)
Geopolymer mortar + PVA	21.5	2.1
Portland-cement-mortar + PVA	23.2	2.5

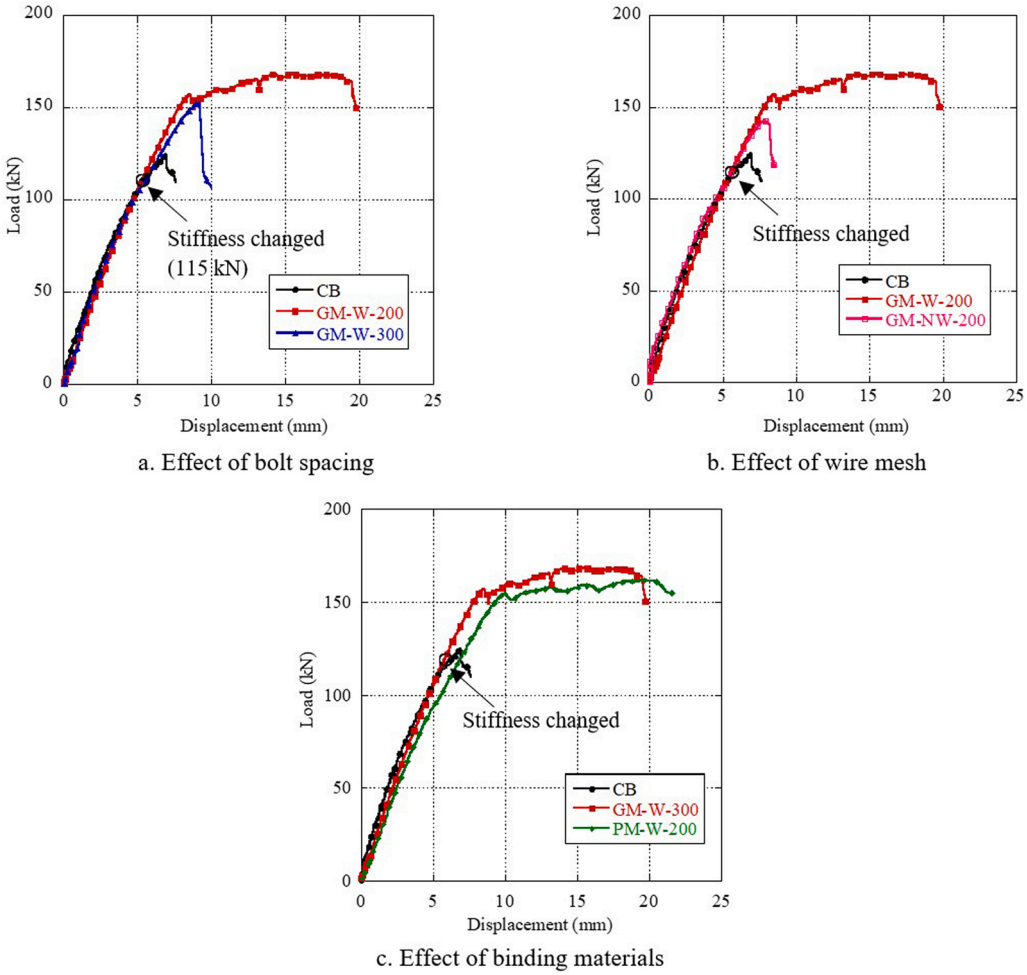

Fig. 6. Load–displacement response.

Table 6
Test results related to test and failure loads.

Specimens	$P_{cr\text{-}panel}$ (kN)	$P_{y\_stirrup}$ (kN)	P_{y_long} (kN)	P_u (kN)	Failure load enhancement (%)	Failure mode
CB	–	–	–	124.8	–	Shear failure
GM-W-200	63.1	165.4	152.4	168.4	34.9	Concrete crushing
GM-W-300	60.7	135.6	153.2	153.2	22.8	Shear + Panel fracture
GM-NW-200	51.5	132.3	142.3	142.3	14.1	Shear + Panel fracture
PM-W-200	87.6	158.5	154.4	161.6	29.5	Concrete crushing

$P_{cr\text{-}panel}$: first crack at the panel, $P_{y\_stirrups}$: yielding load of stirrup, P_{y_long}: yielding load of longitudinal rebars, *and* P_u: failure load.

almost similar in terms of stiffness and load–displacement.

3.3. Failure load

Specimens CB and GM-NW-200 failed in shear, whereas the remaining beams failed owing to the yielding of longitudinal rebars and concrete crushing at the compression zone (except for GM-W-300). Fig. 7 shows the failure-load enhancement of all the beams.

As shown in Fig. 7, the strengthening method in the different beams significantly enhanced the failure load. The beam GM-W-200, which was strengthened with 200 mm anchor-bolt spacing and wire mesh, had the highest strength-enhancement ratio of 34.9% compared to that of CB. Meanwhile, GM-NW-200, which was strengthened with 200 mm anchor bolt spacing and without wire mesh, showed the lowest strength-enhancement ratio rate of 14.1%.

Comparing the failure loads of GM-W-200 and GM-W-300 as an effect of anchor bolt spacing, it was clearly seen that the failure load significantly increased with smaller anchor bolt spacing. The failure load increments of GM-W-200 and GM-W-300 were 34.9% and

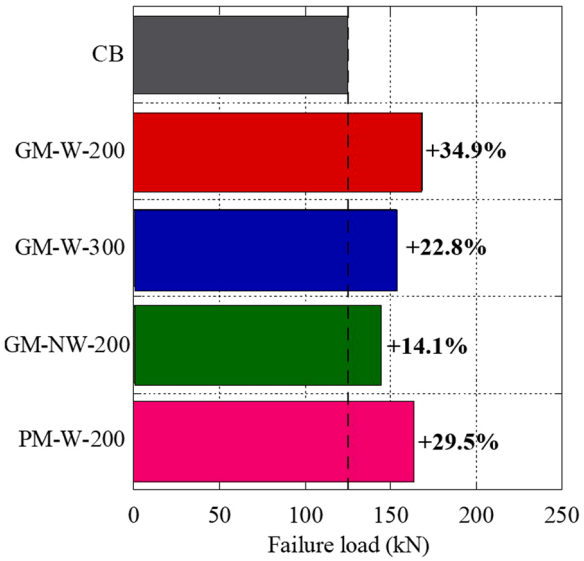

Fig. 7. Failure load and strength enhancement.

22.8%, respectively, compared of the CB. This implies that the anchor bolt spacing is beneficial for improving the shear capacity. The bolt acted as a dowel in transferring the shear force from the RC member to the strengthening panel. With a smaller bolt spacing, the strengthening panel and RC beam work well together, enabling the wire mesh inside the panel to be effectively utilized. This can be observed from the load–strain relationship of the wire mesh, whereas at the same load, the strain in GM-W-200 was greater than that in GM-W-300 (Fig. 8). In addition, the ultimate wire-mesh strain on GM-W-200 was greater than that of GM-W-300. The higher the wire-mesh strain, the higher the contribution of the wire mesh to the increase in shear capacity.

The effect of the wire mesh on the failure load enhancement was evaluated by comparing GM-W-200 and GM-NW-200 with the CB. The GM-W-200 and GM-NW-200 beams were strengthened with an anchor bolt spacing of 200 mm. From Fig. 7, the failure load enhancements of GM-W-200 and GM-NW-200 were 34.9% and 14.1%, respectively, compared to the CB. This implies that the addition of wire mesh to the GMP results in a strength increment of 2.48 times higher than that without the wire mesh. The wire mesh resisted part of the shear load and arrested further crack propagation.

Beams GM-W-200 and PM-W-200 were strengthened using the same anchor bolt spacing (200 mm) and wire mesh but with different binding materials (geopolymer mortar and Portland-cement-mortar). According to Fig. 7, the failure load enhancements of GM-W-200 and PM-W-200 were 34.9% and 29.5%, respectively. This implies that the binding materials had an insignificant effect on

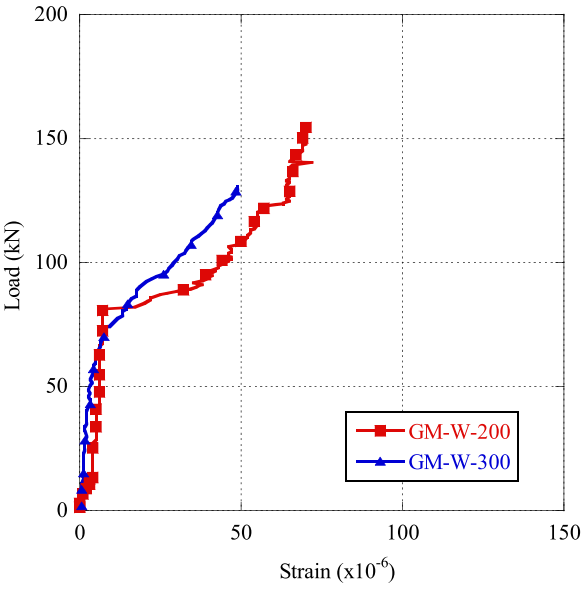

Fig. 8. Load–strain of the transverse-wire mesh.

the shear strength. Therefore, GM can be used as an alternative to Portland cement as the binding material in panels. The use of geopolymers in this study requires the extensive use of thousands of tons of fly-ash waste produced from the coal combustion of power-plant energy in the South Sulawesi Province, Indonesia. At present, the need for eco-friendly materials for sustainable development are a major environmental concern in the construction industry. Compared to OPC, energy consumption and CO_2 emissions during geopolymer production can be significantly reduced, with approximately 80% less CO_2 emissions compared to the production of OPC [7].

Based on the above findings, the GMP with sufficient anchor bolt spacing and wire mesh is an excellent alternative for strengthening structural members in building applications. This is because the GMP was shown to improve the strengthening performance of RC beams in terms of stiffness, post-yielding behavior, maximum load, and failure mode.

3.4. Load–strain response

Three strain gauges were attached to each tested beam to measure the strain progression in the longitudinal rebar, stirrups, and wire mesh. Fig. 9 shows the load-longitudinal–tensile-rebars strain in all beams at midspan. All the longitudinal rebars in the strengthened beam achieved a yielding strain of 2000 $\mu\varepsilon$. However, the longitudinal rebars at the CB did not yield because of shear failure.

The load-stirrup response is shown in Fig. 10. Evidently, at an early stage, the stirrup strains in all the beams linearly increased with the applied load. After diagonal cracks formed at the shear span, the stirrup strain of all the beams increased sharply. Before failure, all the stirrups yielded.

Comparing the strains of the specimens under the same load level, the strain of the strengthened beams GM-W-200 was lower than that of GM-W-300 (Fig. 10). For example, at a load of 125 kN, the stirrup strains at GM-W-200 and GM-W-300 were 500 $\mu\varepsilon$ and 1000 $\mu\varepsilon$, respectively. This indicates that the smaller the anchor bolt spacing, the lower the developed strain in the stirrups. This is because, at the same load level, a higher shear force is shared by the strengthening-panel system in beams with smaller anchor-bolt spacings, which reduces the shear force supported by stirrups and thus leads to a larger reduction in the strain of the stirrups. There was also a good compatibility between the RC beam and panel with a smaller anchor bolt spacing.

The use of a wire mesh at the strengthening panel also affected the stirrup-strain development after the formation of diagonal cracks. According to Fig. 10, the stirrup strain in the strengthened beam with a wire mesh (GM-W-200) was lower than that of the beam without a wire mesh (GM-NW-200). For example, at a load of 125 kN, the stirrup strains at GM-W-200 and GM-W-300 were 500 $\mu\varepsilon$ and 1050 $\mu\varepsilon$, respectively. This implies a contribution of the wire mesh in supporting the shear force along diagonal cracks.

Fig. 11 shows the progression of typical strains in the wire-mesh transverse direction of the strengthening-panel system. The location of the strain gauge at the wire mesh is shown in Fig. 2b. The strains in the transverse-wire mesh were very small prior to the development of diagonal cracks, similar to the progression of strain in the stirrups. Subsequently, there was a significant increase in the wire-mesh strain. In addition, comparing the load level at which the stirrup and wire-mesh strains increased sharply (Figs. 10 and 11), the beginning of the rapid increase in stirrup strain was close to the wire mesh. This implies that the wire mesh supported shear-force sharing. Once the wire mesh supported the carrying load, the propagation of shear cracks was restrained; thus, further strain increases in the stirrups slowed down. This was confirmed from the development of stirrup strains after shear cracking, where the strain at the same load level in GM-W-200 was lower than that in the CB. At the failure load, the wire-mesh strains are approximately 91 $\mu\varepsilon$. Unfortunately, only one strain gauge was attached to the wire mesh. Hence, the strains of the other transverse-wire mesh along the shear span could not be obtained. However, it was confirmed that the effect of wire mesh on the failure load was significant where the failure load was increased from 142.3 kN (GM-NW-200) to 168.4 kN (GM-W-200).

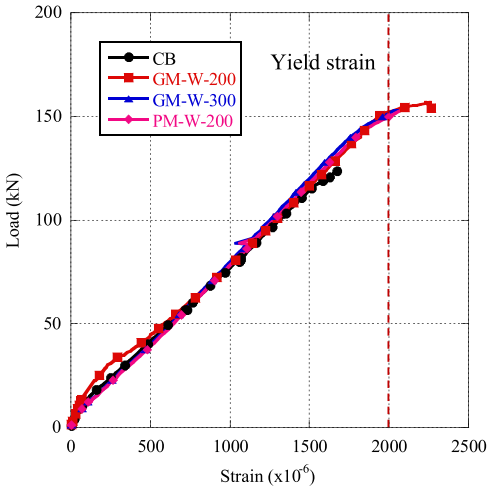

Fig. 9. Load-longitudinal rebar strain.

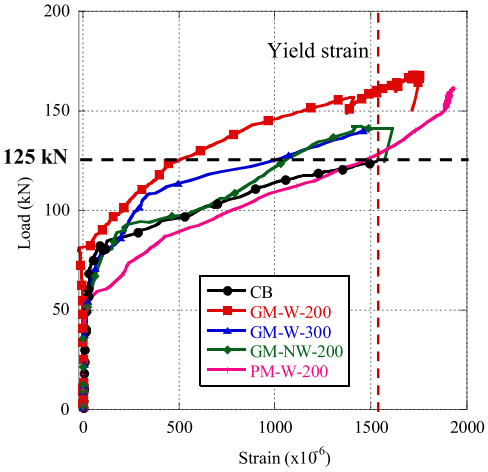

Fig. 10. Load-stirrup strain.

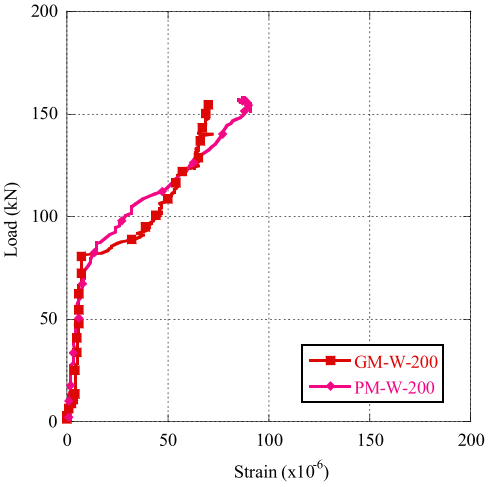

Fig. 11. Load-wire-mesh strain.

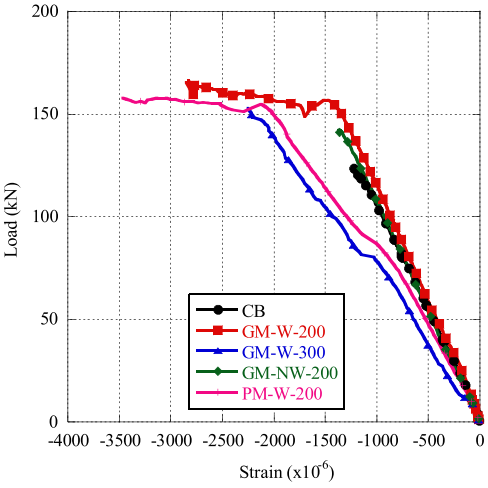

Fig. 12. Load-concrete strain.

Fig. 12 shows the load–strain behavior of the concrete at the outer-compression zone. All beams experienced an increase in strain linear to the applied load. Based on the maximum strain of the concrete at failure, only GM-W-200 and PM-W-200 reached the ultimate strain of the concrete (ε_{cu}). This indicated that the strengthening panels with an anchor spacing of 200 mm and wire mesh provided the ideal behavior for RC beams that fail because of under-reinforced conditions.

3.5. Crack pattern

Fig. 13 shows the crack patterns of the CB. Flexural cracks occurred at 37.8 kN around the constant-moment region. At 56 kN, the first crack in the shear span initially opened on the bottom side. Some cracks extended to diagonal cracks at further load levels. After the main diagonal cracks opened and propagated to the loading point, another diagonal crack appeared over the main cracks at 94.6 kN. The strut between these two diagonal cracks was assumed to be in compression after the main diagonal crack occurred.

The crack patterns of the strengthened beams are shown in Figs. 14–17. In these figures, the geopolymer–mortar panels are shown in blue, whereas the Portland-cement-mortar panels are shown in green. The flexural crack first opened in the constant-moment region, followed by flexural cracks in the strengthening panels. In the beam without the wire mesh GM-NW-200, the diagonal crack propagated towards the loading point, as shown in Fig. 16. At failure, only GM-W-200 and PM-W-200 failed because of concrete crushing in the compression zone. Meanwhile, the strengthened beam with a 300 mm anchorage spacing (GM-W-300) and without wire mesh (GM-NW-200) failed with the same brittle failure as the CB. This demonstrates that an anchor spacing of 200 mm and wire mesh played an important role in changing the failure pattern from brittle to ductile.

The spacing between the anchor bolts of 300 mm also caused anchorage failure at the panel owing to stress localization in that area (Fig. 15**c**). As a result, there was a separation of 10 mm between the panels and concrete. This indicates that the applied stress at the anchor was greater than the resisted stress at each anchor bolt. This phenomenon was not observed in the GMP with an anchor spacing of 200 mm.

In addition, the crack width at the strengthening panels was measured using a crack meter immediately after failure. Fig. 18**(a, b)** compare the crack widths of panels with and without wire mesh. The results show that the panel with wire mesh has a much smaller crack width (0.4–1.4 mm) than that without wire mesh (3.2 mm). This demonstrates that the wire mesh significantly influences the crack width and propagation in the panels.

After the test, the strengthening panel was removed to observe the crack pattern in the shear span of the RC beam. Figs. 14–17 present a comparison of the crack patterns of beams on the panel and RC sides. The results show that diagonal cracks propagate along the support and loading points in all specimens. This contrasted with the observation on the panel side, where diagonal cracks were not observed, except in the specimen without a wire mesh (GM-NW-200). This indicates that the strengthening panels with wire mesh effectively inhibited the rate of diagonal crack development on the RC side and delayed the occurrence of shear failure, as occurs in beams without a wire mesh.

4. Failure mechanisms

4.1. Shear failure of RC beams strengthened by the GMP

The loading test of the strengthened beams showed the same failure pattern in the panel with an anchor-bolt spacing of 300 mm (GM-W-300) as that without a wire mesh (GM-NW-200). The behavior of specimen GM-W-300 was used to reveal the failure mechanism. The load–displacement relationship of GM-W-300 is shown in Fig. 19. Initial flexural cracking appeared under the loading point

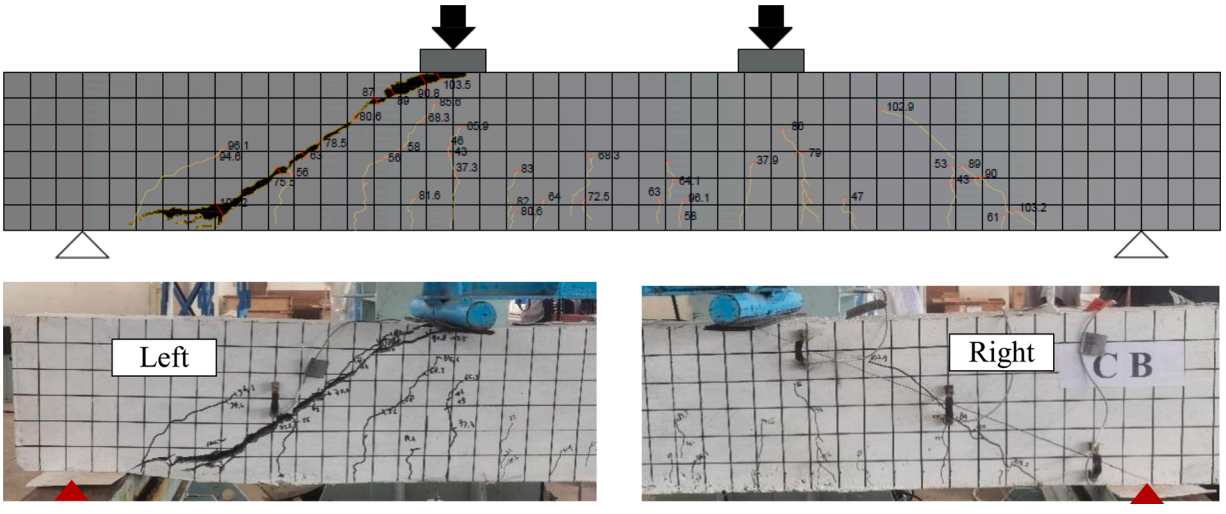

Fig. 13. Crack pattern of the control beam (CB).

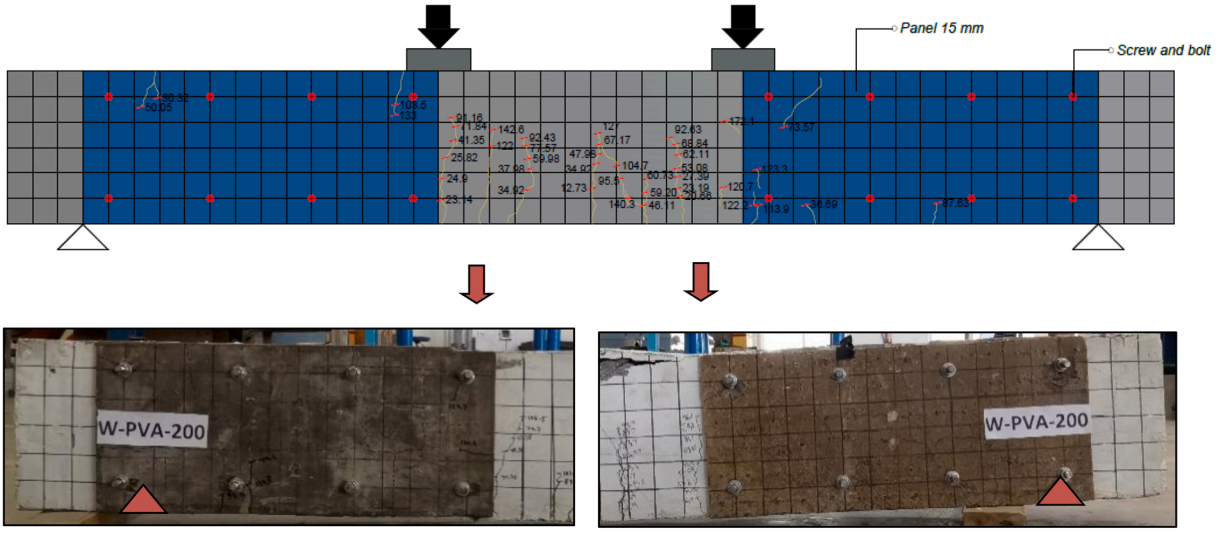

a. Panel side (before removing the panels)

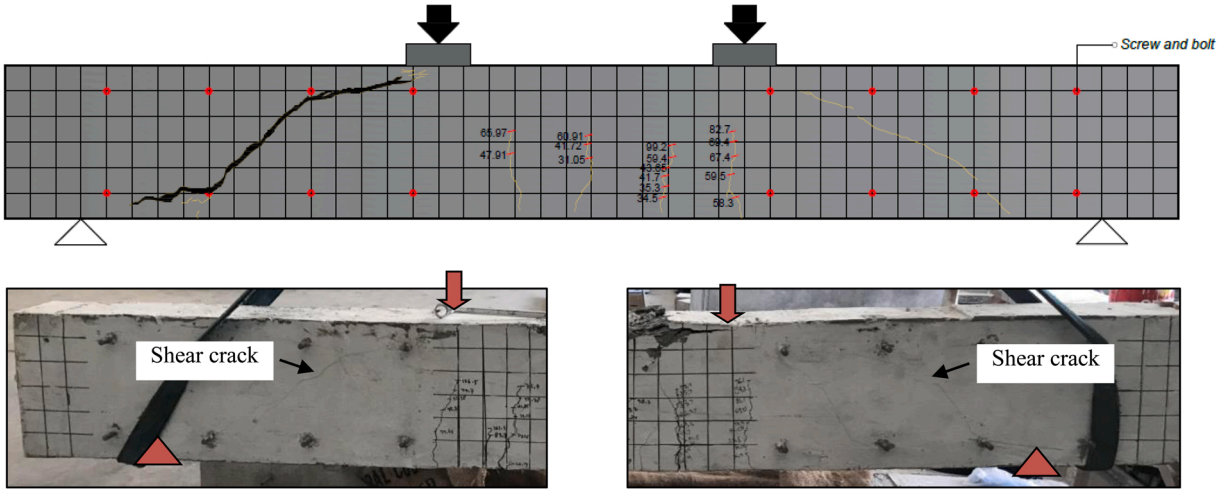

b. RC side (after removing the panels)

Fig. 14. Crack pattern of GM-W-200.

in the constant-moment region of the RC beam at a load of 22.7 kN. The first cracking on the GMP was observed at a load of 60.70 kN. The stiffness changed and propagation cracks were observed on both sides of the shear span. The separation between the RC and GMP was first observed at approximately 68.0 kN, as shown in the gap at the interface (Fig. 20).

A diagonal crack on the GMP occurred at a load of 84.5 kN at the stirrups yielded at a load of 135.6 kN (Fig. 21). Subsequently, flexural cracks on the beam side propagated vertically near the neutral axis. When the load reached 153.2 kN with a deflection of 9.1 mm, the load dropped drastically. Based on the strain observations shown in Fig. 21, the longitudinal rebars reached the yield strain. All the concrete on the outer-compression side was not crushed. This was confirmed from the load-concrete strain in Fig. 21, where the concrete strain was still much lower than the ultimate strain of the concrete ($\varepsilon_{cu} = 3000\ \mu\varepsilon$). Hence, a sudden failure occurred immediately after yielding of the longitudinal rebars. The strengthening panels can no longer carry shear forces after the longitudinal rebars have yielded; therefore, the beam loses its capacity to resist the load. The panels at the failure load were found to fracture vertically under the loading point (Fig. 22).

4.2. Flexural failure of RC beams strengthened by the GMP

From the loading test, the failure patterns of GM-W-200 and PM-W-200 were similar. That is, both strengthened beams failed because the longitudinal rebars that yielded before the concrete at the compression side were crushed. The behavior of specimen GM-

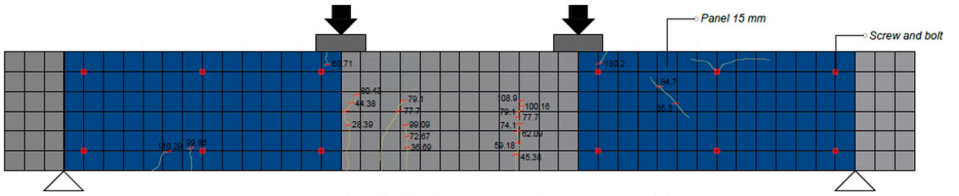

a. Panel side (before removing the panels)

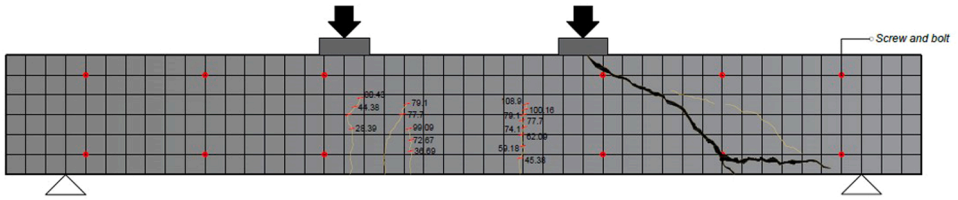

b. RC side (after removing the panels)

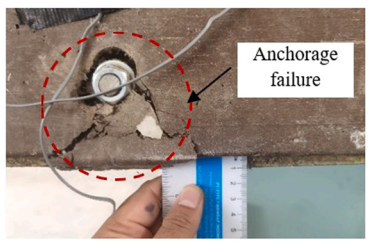

c. Anchorage failure and separation between the GMP and RC

Fig. 15. Crack pattern of GM-W-300.

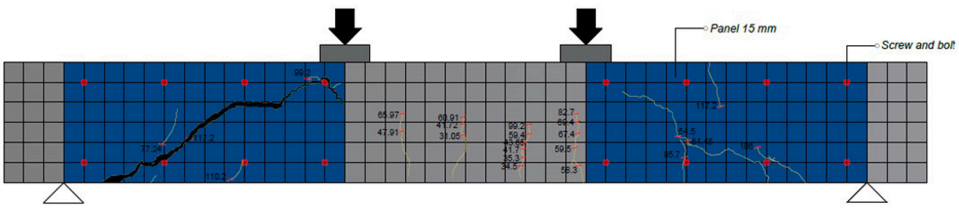

a. Panel side (before removing the panels)

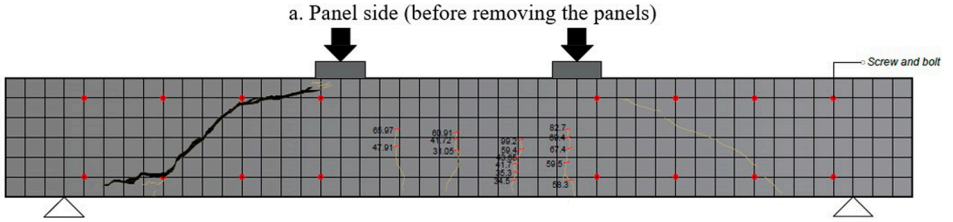

b. RC side (after removing the panels)

Fig. 16. Crack pattern of PM-W-200.

W-200 was used to explain this failure mechanism. The load–displacement relationship of GM-W-200 is shown in Fig. 23. The loads and strains of the longitudinal rebars, stirrups, and concrete are illustrated in Figs. 9, 10, and 12, respectively.

The initial flexural cracking first appeared in the constant-moment region of the RC beam at a load of 25.2 kN. The first flexural cracking on the GMP was observed at 63.1 kN. A diagonal crack at the shear span occurred at 80.8 kN, which was noticed from the slight increase in the stirrup strain (Fig. 10). The separation between the RC and GMP occurred at approximately 67.4 kN as shown by the gap between the panel and RC-beam interface (Fig. 24). The load suddenly dropped when it reached 152.4 kN; thereafter, it continued to increase gradually. Based on the strain observations, the longitudinal rebar at this point reached the yield strain. As the load increased, the stirrup yielded at 163.2 kN. The load still increased gradually, but was not proportional to the displacement owing to the contribution of the strengthening-panel systems. Finally, the beam failed at a load of 168.4 kN due to concrete crushing in the

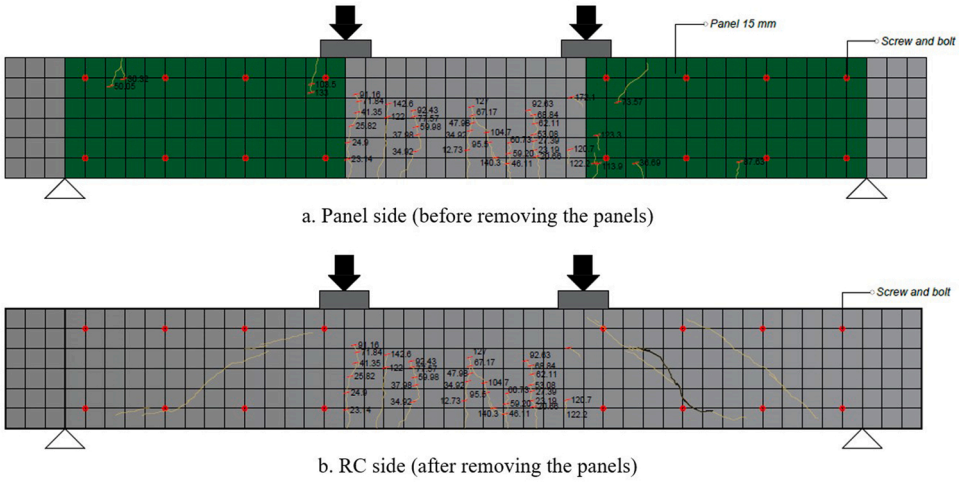

Fig. 17. Crack pattern of PM-W-200.

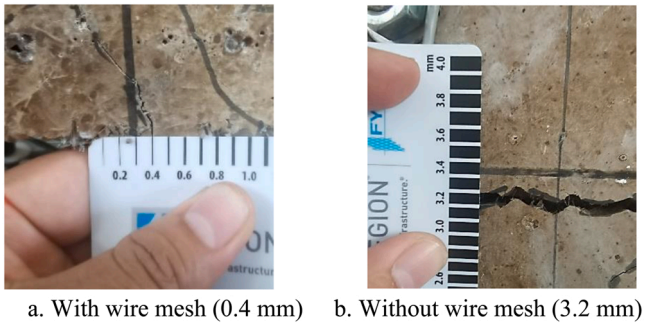

Fig. 18. Effect of wire mesh on crack width.

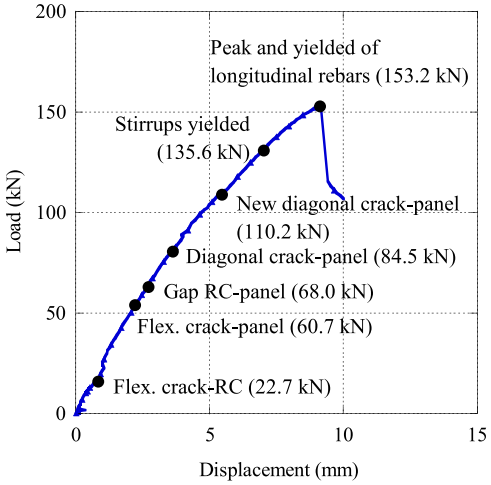

Fig. 19. Load–displacement of GM-W-300.

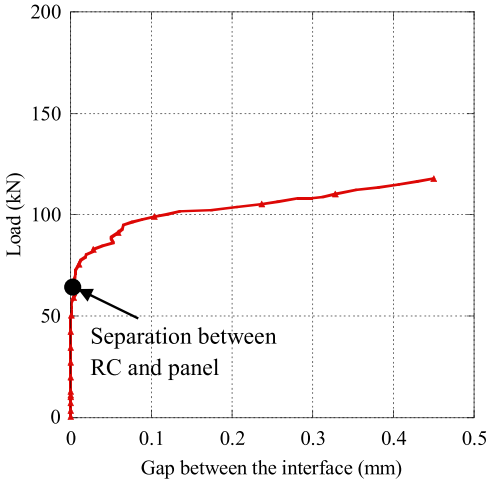

Fig. 20. Gap at interface of GM-W-300.

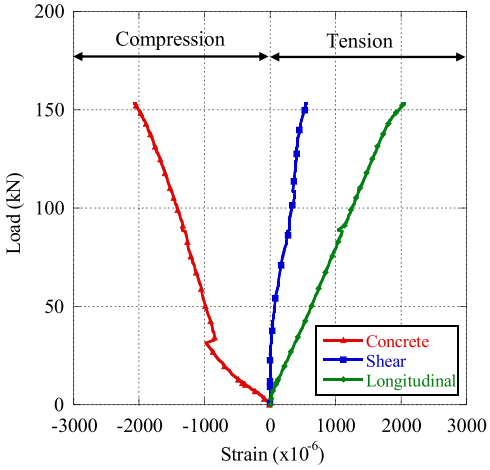

Fig. 21. Load–strain of GM-W-300.

compression zone (Fig. 25). The results show that the wire mesh on the strengthening panels changed the failure mode of the beams from shear to flexural failure.

5. Prediction of the shear capacity carried by the GMP

The prediction of shear capacity carried by the GMP with and without wire mesh was proposed using force equilibrium along the section of diagonal cracks, as shown in Fig. 26(a, b). The shear-carrying capacity was half of the failure mode ($V = P/2$) owing to the four-point bending test. Baghi et al. [47] developed a similar design approach based on simplified-modified–compression-field theory (SMCFT).

According to the free-body diagram in Fig. 26a, the shear capacity of RC beams strengthened with the GMP, and wire mesh is given by Eq. (2). The contributions from the concrete (v_c) and stirrups (v_s) in the RC beam, and from the panel (v_{panel}) and wire mesh (v_{wire}) need to be recognized to complete the equilibrium condition in Eq. (2). However, for a beam without a wire mesh (Fig. 26b), the contribution of $v_{wire} = 0$ is as expressed in Eq. (3).

$$v = v_c + v_s + v_{panel} + v_{wire} \tag{2}$$

$$v = v_c + v_s + v_{panel} \tag{3}$$

The expressions for v_c and v_s are presented in Eqs. (4) and (5), respectively:

$$v_c = \beta\sqrt{f'_c}, \tag{4}$$

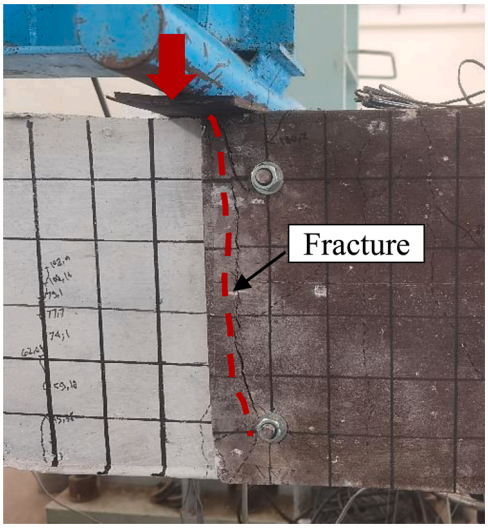

Fig. 22. Fracture of the panel.

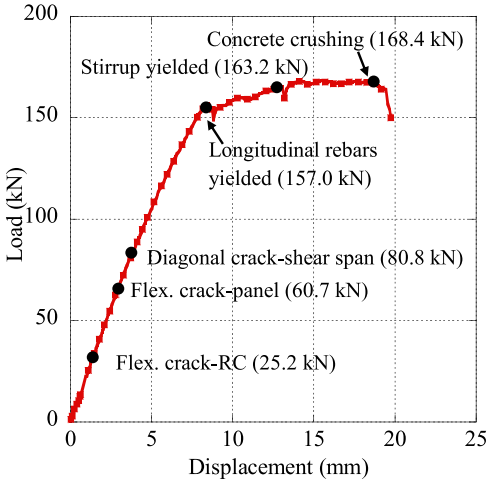

Fig. 23. Load–displacement of GM-W-200.

$$v_s = \rho_{st} f_{st.y} cot\theta, \tag{5}$$

where v_c and v_s are the shear strengths of concrete and stirrups, respectively. Moreover, f'_c, ρ_{st}, and $f_{st.y}$ are the compressive strength of concrete (MPa), stirrup ratio, and yield stress of the stirrups (MPa), respectively. Bentz et al. [48] developed an SMCFT, where the shear strength is a function of two parameters, namely, the tensile-stress factor in the cracked concrete (β) and the inclination of the diagonal-compressive stress in the web of the section (θ), as stated in Eqs. (6) and (7):

$$\beta = \frac{0.4}{1 + 1500\varepsilon_{sl}} \frac{1300}{1000 + S_{xe}}, \tag{6}$$

$$\theta = (29 + 700\varepsilon_{sl}).\left(0.88 + \frac{s_{xe}}{2500}\right) \leq 75^o. \tag{7}$$

In Eqs. (6) and (7), ε_{sl} is the longitudinal strain assessed at the mid-depth of the beam cross-section, whereas S_{xe} is the crack-spacing parameter, obtained using Eqs. (8) and (9), respectively.

$$\varepsilon_{sl} = \frac{f_{sx}}{E_s} = \frac{v.cot\theta - v_c/cot\theta}{E_s \rho_{sx}} \tag{8}$$

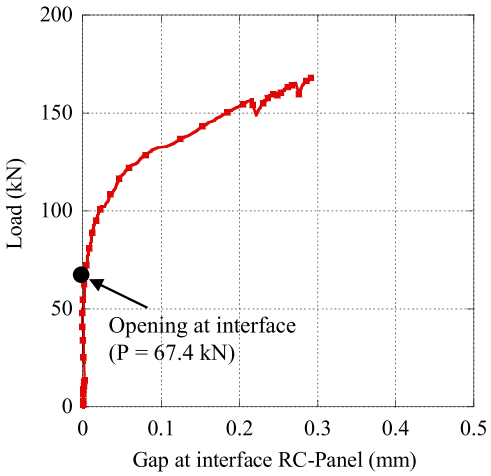

Fig. 24. Gap at interface of GM-W-200.

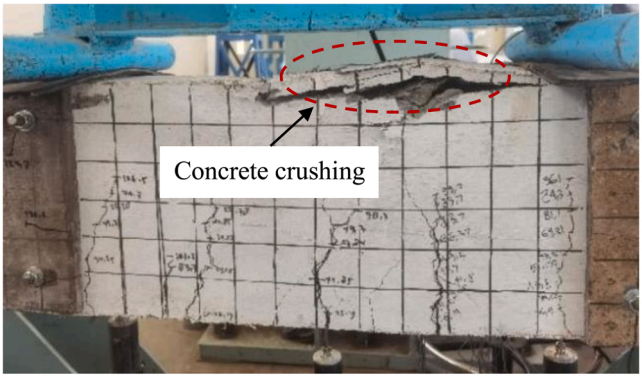

Fig. 25. Concrete crushing at the compression zone.

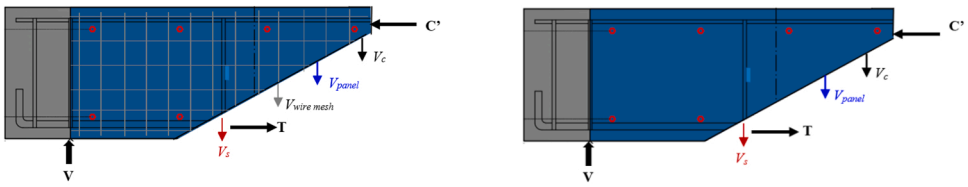

Fig. 26. Free-body diagram of the strengthened beam.

$$S_{xe} = \frac{35 s_x}{a_g + 16} \geq 0.85 s_x \tag{9}$$

Here, s_x and a_g denote the yield strain of the longitudinal reinforcement (Fig. 26) and the maximum size of the aggregate, respectively. In Eqs. (8) and (9), E_s, ρ_{sx}, and ε_x are the modulus of elasticity (MPa), reinforcement ratio, and yield strain of the longitudinal reinforcement, respectively, and ρ_{sl} is obtained using Eq. (10):

$$\rho_{sl} = \frac{A_{sl}}{A_c}, \tag{10}$$

where A_{sl} and A_c is the cross-sectional area of the longitudinal rebar and concrete, respectively.

According to Blanksvärd [49], the maximum shear stress in a rectangular-noncracked section is defined by Eq. (11):

$$\tau_{max} = \frac{VQ}{It} = \frac{3V}{2A}, \tag{11}$$

where V denotes the total shear force; Q and I are the first and second moments of the area, respectively; and t is the thickness of the cross-sectional area. The shear resistance of the panels is obtained by determining the existence of a complete bond between the GMP and concrete substrate as follows:

$$V_{panel} = 2\left(2/3 t_{panel} h_{panel} \tau_{avg}\right), \tag{12}$$

where t_{panel} is the panel thickness (15 mm) and h_{panel} is the height of the panel (300 mm). Note that Factor 2 originates from the plates applied on both sides of the beam. The τ_{avg} is the average shear stress of the panel, and according to the results presented in [50], this value is assumed as 3.5 MPa. Subsequently, complete bond conditions between the GMP and the concrete substrate are expected. Based on Eq. (12), the contribution of the panel to the shear strength (v_{panel}) is given by Eq. (13):

$$v_{panel} = 2\left(2/3 t_{panel} h_{panel} \tau_{avg}\right) b * w.d. \tag{13}$$

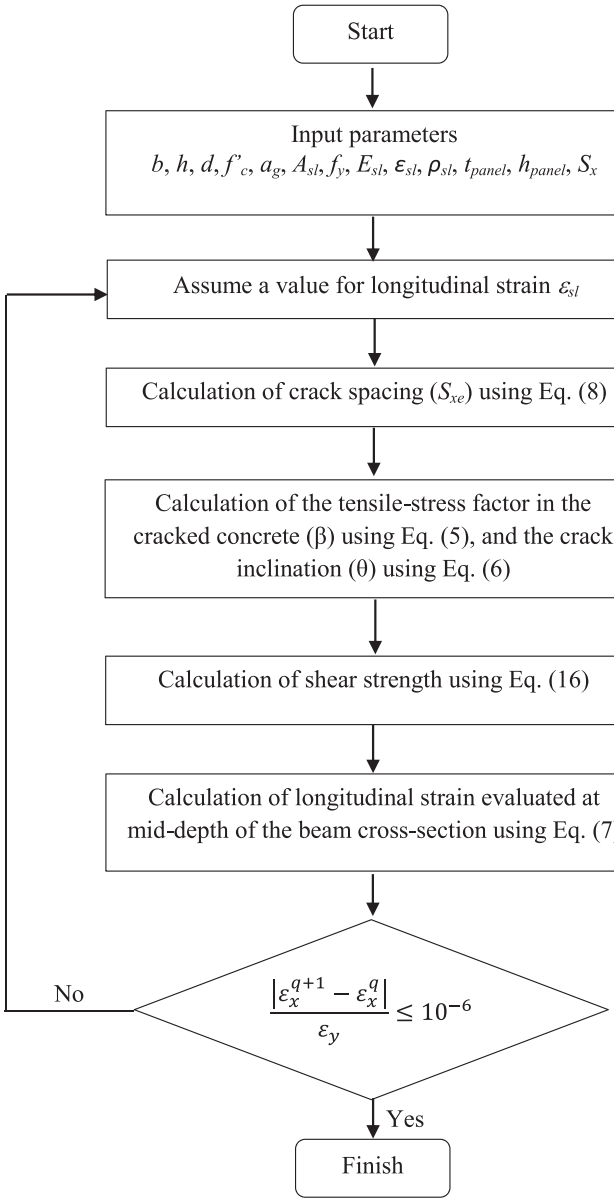

Fig. 27. Estimation procedure of BSMCFT implemented to strengthen the panel.

For beams strengthened with the GMP and mechanical anchors, the base width of the concrete-semi–pyramidal-tensile fracture (b^*_w) was taken as $b^*_w = (b_w+2t_{panel})/2$. Accordingly, the contribution of the panel to shear strength was calculated using Eq. (14):

$$v_{panel} = \frac{4t_{panel}h_{panel}\tau_{avg}}{3(2b^*_w)d}. \tag{14}$$

To evaluate the contribution of the wire mesh to the shear strength (v_{wire}), the prediction model proposed by Escrig [51] was developed. According to Escrig [51], the contribution of the longitudinal-wire mesh can be ignored ($\alpha = 90^o$). Therefore, only the wire mesh in the transverse direction was applied in this study and is predicted by the following formula:

$$v_{wire} = \rho_{wire}\varepsilon_{wire}E_{wire}, \tag{15}$$

where ρ_{wire}, E_{wire}, and ε_{wire} are the reinforcement ratios of the transverse-wire mesh, elastic modulus of the wire mesh (200,000 MPa in this study), and effective strain in the wire mesh, respectively. The value of ε_{wire} was obtained from experiments.

Accordingly, the shear strength of an RC beam strengthened with the GMP, and wire mesh is defined by Eq. (16) by recognizing the contributions of the concrete, stirrups, panels, and wire mesh.

$$v = v_c + v_s + v_{panel} + v_{wire} = \beta\sqrt{f'_c} + v_s + \rho_{st}f_{st.y}\cot\theta + \frac{4t_{panel}h_{panel}\tau_{avg}}{3(2b^*_w)d} + \rho_{wire}\varepsilon_{wire}E_{wire} \tag{16}$$

For the beam without the wire mesh, the contribution of the wire mesh to the shear strength is $v_{\text{wire}} = 0$. Therefore, Eq. (16) was modified, as expressed in Eq. (17):

$$v = v_c + v_s + v_{panel} = \beta\sqrt{f'_c} + v_s + \rho_{st}f_{st.y}\cot\theta + \frac{4t_{panel}h_{panel}\tau_{avg}}{3(2b^*_w)d} \tag{17}$$

The shear strength value in each contribution was multiplied by the beam width (bw) and effective depth (d) to calculate the shear capacity.

By following the procedures presented in Fig. 27, a method to calculate the shear strength of the RC beams according to the SMCFT is shown. This solution is adapted to the strengthening panel in this study. The results are summarized in Table 7.

Table 7 summarizes the experimental results and predicted values according to the analytical formulations. The shear-capacity ratio between the experimental and analytical predictions ($V_{exp}/V_{analysis}$) was 1.02 with a COV of 3.5%. The results in this table show that the analytical approach can accurately predict the ultimate shear capacity of RC beams, which have been strengthened using the GMP. The SMCFT model can be adopted for beam-shear strengthened members using composite laminates or panels. The same model was adopted by Lourenço et al. [46] and Baghi et al. [47], where the results showed a high level of prediction accuracy.

6. Conclusions

This study analyzed the performance of three shear-strengthened beams with the GMP, one shear-strengthened beam with a Portland-cement-mortar panel, and one CB. Anchor-bolt spacing, wire-mesh existence, and binding-material types were examined. The following conclusions are drawn from the experimental and analytical results:

1. GMPs can effectively enhance the shear capacities of RC beams. All the beams exhibited a shear strength enhancement of 14.1% (a GMP without a wire mesh) to 34.9% (a GMP with a wire mesh) compared to the control beam.
2. The effect of the wire mesh on the GMP was greater than that of the anchor bolt spacing. The shear capacity of the beam with an anchor spacing of 300 mm (GM-W-300) was reduced by 15.5% when compared to beam GM-W-200, while the shear capacity of the beam without wire mesh (GM-NW-200) was reduced by 9.0%. This was because the wire mesh resisted part of the shear load and arrested any further crack propagation.

Table 7
Comparison between the experimental and analytical results.

Specimen	V_{exp} (kN)	$V_{analysis}$ (kN)					$V_{exp}/V_{analysis}$
		V_c	V_s	V_{panel}	$V_{wire\ mesh}$	V_{tot}	
CB	62.38	37.25	24.03	0.00	0.00	61.27	1.02
GM-W-200	84.19	27.16	23.72	10.00	17.46	78.34	1.07
GM-W-300	76.61	27.16	23.72	10.00	17.46	78.34	0.98
GM-NW-200	71.17	28.82	23.87	18.00	0.00	70.69	1.01
PM-W-200	80.80	27.16	23.72	10.00	17.46	78.34	1.03
Average							1.02
CoV (%)							3.5

3. RC beams strengthened with the GMP experienced shear failure when insufficient bolt spacing or no wire mesh is present. However, if the anchor-bolt spacing is sufficient and the wire mesh is provided at the GMP, the failure mode changes from shear to flexural failure.
4. The binding materials had a minor effect on the shear capacity and failure mode because the strengths of the GMP and Portland-cement-mortar panels were similar. Because the failure load and mode were identical, the GM can be used as an alternative material in strengthening panels.
5. An analytical calculation adopted from the SMCFT was used to estimate the shear capacity of the RC beam strengthened with the GMP. The results indicated that the calculated shear capacity correlated with the experiments, where the shear-capacity ratio between the experimental and analytical predictions ($V_{exp}/V_{analysis}$) was 1.02 with a COV of 3.5%.

Declaration of Competing Interest

The authors declare the following financial interests/personal relationships which may be considered as potential competing interests: This research is funded by Ministry of Research, technology and Higher Education of Indonesian Government for their financial support (Contract No 8044/UN4.1.2.3/PL.02.00 /2021). The authors declare that all published data has obtained permission from the funder.

Data availability

Data will be made available on request.

Acknowledgment

The authors are grateful to the Ministry of Research, Technology and Higher Education of Indonesian Government for their financial support (Contract No. 8044/UN4.1.2.3/PL.02.00 /2021).

References

[1] J.P. Firmo, J.R. Correia, L.A. Bisby, Fire behaviour of FRP-strengthened reinforced concrete structural elements: A state-of-the-art review, Compos B 80 (2015) 198–216.
[2] A. Peled, Confinement of damaged and non-damaged structural concrete with FRP and TRC sleeves, J. Compos Constr. 11 (5) (2007) 514–522.
[3] J. Davidovits, Geopolymers: inorganic polymeric new materials, J. Therm. Anal. Calor. 37 (8) (1991) 1633–1656.
[4] P. Duxson, J.L. Provis, G.C. Lukey, et al., The role of inorganic polymer technology in the development of green concrete, Cem. Concr. Res 37 (12) (2007) 1590–1597.
[5] M.N. Hadi, H. Zhang, S. Parkinson, Optimum mix design of geopolymer pastes and concretes cured in ambient condition based on compressive strength, setting time and workability, J. Build. Eng. 23 (2019) 301–313.
[6] W.H. Lee, J.H. Wang, Y.C. Ding, T.W. Cheng, A study on the characteristics and microstructures of GGBS/FA based geopolymer paste and concrete, Constr. Build. Mater. 211 (2019) 807–813.
[7] P. Saranya, P. Nagarajan, A.P. Shashikala, Performance evaluation of geopolymer concrete beams under monotonic loading, in: Structures, 20, Elsevier, 2019, pp. 560–569.
[8] A.M. Zeyad, H.M. Magbool, B.A. Tayeh, A.R.G. Azevedo, A. Abutaleb, Q. Hussain, Production of geopolymer concrete by utilizing volcanic pumice dust, Case Stud. Constr. Mater. 16 (2022), e00802.
[9] N.S. Yacob, M.A. ElGawady, L.H. Sneed, A. Said, Shear strength of fly ash-based geopolymer reinforced concrete beams, Eng. Struct. 196 (2019), 109298.
[10] T. Srividya, R.P.R. Kannan, M. Sivasakthi, A. Sujitha, R. Jelayakshmi, A state-of-the-art on development of geopolymer concrete and its field applications, Case Stud. Constr. Mater. 16 (2022), e00812.
[11] A.L. Almutairi, B.A. Tayeh, A. Adesina, H.T. Isleem, A.M. Zeyad, Potential applications of geopolymer concrete in construction: A review, Case Stud. Constr. Mater. 15 (2021), e00733.
[12] F.A.-Z. Refaie, R. Abbas R, F.H. Fouad, Sustainable construction system with Egyptian metakaolin based geopolymer concrete sandwich panels, Case Stud. Constr. Mater. 13 (2020), e00436.
[13] R.S. Fediuk, M. Science, Mechanical Activation of Construction Binder Materials by Various Mills Mechanical Activation of Construction Binder Materials by Various Mills, 2016.
[14] M.T. Marvila, A.R.G. Azevedo, L.B. OIliveora, G.C. Xavier, C.M.F. Vieira, Mechanical, physical and durability properties of activated alkali cement based on blast furnace slag as a function of $\%Na_2O$, Case Stud. Constr. Mater. 15 (2021), e00723.
[15] P. He, D. Jia, T. Lin, M. Wang, Y. Zhou, Effects of high-temperature heat treatment on the mechanical properties of unidirectional carbon fiber reinforced geopolymer composites, Ceram. Int. 36 (4) (2010) 1447–1453.
[16] D.P. Dias, C. Thaumaturgo, Fracture toughness of geopolymeric concretes reinforced with basalt fibres, Cem. Concr. Compos 27 (2005) 49–54.
[17] S.F.U. Ahmed, M. Maalej, P. Paramasivam, Flexural responses of hybrid steel-polyethylene fibre reinforced cement composites containing high volume fly ash, J. Constr. Build. Mater. 21 (5) (2006) 1088–1097.
[18] J.L. Provis, Geopolymers and other alkali activated materials: why, how, and what? Mater. Struct. Constr. 47 (2014) 11–25.
[19] Yazan Alrefaei, Jian-Guo Dai, Tensile behavior and microstructure of hybrid fiber ambient cured one-part engineered geopolymer composites, Constr. Build. Mater. 184 (2018) 419–431.
[20] Y. Zhang, W. Sun, Z. Li, Impact behaviour and microstructural characteristics of PVA fibre reinforced fly ash geopolymer boards prepared by extrusion technique, J. Mater. Sci. 41 (2006) 2787–2794.
[21] Y. Zhang, W. Sun, Z. Li, Eddie, C. Chungkong, Impact properties of geopolymer based extrudates incorporated with fly ash and PVA short fibre, Constr. Build. Mater. 22 (2008) 370–383.
[22] Y. Zhang, W. Sun, Z. Li, X. Zhou, Geopolymer extruded composites with incorporated fly ash and polyvinyl alcohol short fibre, Acids Mater. J. 106 (1) (2009) 3–10.
[23] F. Puertas, T. Amat, A. Fernandez-jimenez, T. Vazquez, Mechanical and durable behaviour of alkaline cement mortars reinforced with polypropylene fibres, Cem. Concr. Res 33 (2003) 2031–2036.
[24] N. Behzad, S. jay, U.A.S. Faiz, Tensile Strain Hardening Behavior of PVA Fiber-Reinforced Engineered Geopolymer Composite, J. Mater. Civ. Eng. (2015). ASCE, 04015001-1-04015001-12.

[25] Yazan Alrefaei, Jian-Guo Dai, Tensile behavior and microstructure of hybrid fiber ambient cured one-part engineered geopolymer composites, Constr. Build. Mater. 184 (2018) 419–431.
[26] T. Alomayri, F.U.A. Shaikh, I.M. Low, Thermal and mechanical properties of cotton fabric-reinforced geopolymer composites, J. Mater. Sci. 48 (19) (2013) 6746–6752.
[27] B. Nematollahi, J. Sanjayan, J.X.H. Chai, T.M. Lu, Properties of fresh and hardened glass fiber reinforced fly ash based geopolymer concrete, Key Eng. Mater. 594–595 (2014) 629–633.
[28] M. Alzeer, K. MacKenzie, Synthesis and mechanical properties of novel composites of inorganic polymers (geopolymers) with unidirectional natural flax fibers (Phormium tenax), Appl. Clay Sci. 75 (2013) 148–152.
[29] T. Lin, D. Jia, P. He, M. Wang, D. Liang, Effects of fiber length on mechanical properties and fracture behavior of short carbon fiber reinforced geopolymer matrix composites, Mater. Sci. Eng. A 497 (1) (2008) 181–185.
[30] K. Vijai, R. Kumuthaa, B. Vishnuramb, Effect of inclusion of steel fibres on the properties of geopolymer concrete composites, Asian J. Civ. Eng. 13 (3) (2012) 377–385.
[31] T.S. Ng, A. Amin, S.J. Foster, The behaviour of steel-fibre reinforced geopolymer concrete beams in shear, Mag. Concr. Res 65 (5) (2013) 308–318.
[32] S. Bernal, R.D. Gutierrez, S. Delvasto, E. Rodriguez, Performance of an alkali- activated slag concrete reinforced with steel fibres, Constr. Build. Mater. 24 (2010) 208–214.
[33] S. Ahmed, M. Maalej, Tensile strain hardening behaviour of hybrid steel poly ethylene fibre reinforced cementitious composites, Constr. Build. Mater. 23 (1) (2009) 96–106.
[34] Yazan Alrefaei, Jian-Guo Dai, Tensile behavior and microstructure of hybrid fiber ambient cured one-part engineered geopolymer composites, Constr. Build. Mater. 184 (2018) 419–431.
[35] J.J. Ekaputri, C. Fujiyama, N. Chijiwa, T.D. Ho, H.T. Nguyen, Improving Geopolymer Characteristics with Addition of Poly-Vinyl Alcohol (PVA) Fibers, Civ. Eng. Dimens. Vol. 23 (No. 1) (2021) 28–34.
[36] M.H. Al-Majidi, A.P. Lampropoulos, A.B. Cundy, O.T. Tsioulou, S. Alrekabi, Flexural performance of reinforced concrete beams strengthened with fibre reinforced geopolymer concrete under accelerated corrosion, Structures Volume 19 (2019) 394–410.
[37] W.D. Salman, A.A. Mansor, Fibrous geopolymer paste composites for nearsurface-mounted strengthening of reinforced concrete beams in flexure, Case Stud. Constr. Mater. 14 (2021), e00529.
[38] E.J. Guades, H. Stang, J.W. Schmidt, G. Fischer, Flexural behavior of hybrid fibre-reinforced geopolymer composites (FRGC)-jacketed RC beams, Eng. Struct. 235 (2021), 112053.
[39] S.M. Laskar, S. Talukdar, A study on the performance of damaged RC members repaired using ultra-fine slag based geopolymer mortar, Constr. Build. Mater. 217 (2019) 216–225.
[40] S.M. Laskar, S. Talukdar, Slag-Based Geopolymer Concrete as Reinforced Concrete Jacketing Agent, J. Mater. Civ. Eng. 33 (7) (2021), 04021150.
[41] F. Bencardino, A. Condello, Eco-friendly external strengthening system for existing reinforced concrete beams, Compos. Part B Eng. 93 (2016) 163–173.
[42] E. Vasconcelos, S. Fernandes, J.L. Barroso de Aguiar, F. acheco-Torgal, Concrete retrofitting using metakaolin geopolymer mortars and CFRP, Constr. Build. Mater. 25 (8) (2011) 3213–3221.
[43] T. Phoo-Ngernkham, V. Sata, S. Hanjitsuwan, C. Ridtirud, S. Hatanaka, P. Chindaprasirt, High calcium fly ash geopolymer mortar containing Portland cement for use as repair material, Constr. Build. Mater. 98 (2015) 482–488.
[44] H.Y. Zhang, J. Yan, V. Kodur, L. Cao, Mechanical behavior of concrete beams shear strengthened with textile reinforced geopolymer mortar, Eng. Struct. 196 (2019), 109348.
[45] P. Limpaninlachat, T. Nakamura, K. Kono, J. Niwa, Shear Strengthening Performance of Post-tensioned UFC Panel on Reinforced Concrete Beams, J. Adv. Concr. Technol. Vol. 15 (2017) 558–573.
[46] L. Lourenço, Z. Zamanzadeh, J.A.O. Barros, M. Rezazadeh, Shear strengthening of RC beams with thin panels of mortar reinforced with recycled steel fibres, J. Clean. Prod. 194 (2018) 112–126.
[47] H. Baghi, J.A.O. Barros, F. Menkulasi, Shear strengthening of reinforced concrete beams with Hybrid Composite Plates (HCP) technique: Experimental research and analytical mode, Eng. Struct. 125 (2016) 504–520.
[48] E.C. Bentz, F.J. Vecchio, M.P. Collins, Simplified modified compression field theory for calculating shear strength of reinforced concrete elements, Acids Struct. J. 103 (4) (2006) 614–624.
[49] T. Blanksvärd, Strengthening of concrete structures by the use of mineral-based composites, PhD Thesis. Luleå University of Technology, Luleå, Sweden, 2009.
[50] D.M.J. Sumajouw, D. Hardjito, S. Wallah, B.V. Rangan, Behavior of geopolymer concrete columns under equal load eccentricities, Acids Spec. Publ. 228 (2005) 577–594.
[51] C. Escrig, L. Gil, E. Bernat-Maso, et al., Experimental and analytical study of reinforced concrete beams shear strengthened with different types of textile-reinforced mortar, Constr. Build. Mater. 83 (2015) 248–260.